Electr Eng (2018) 100:1601–1612
https://doi.org/10.1007/s00202-017-0638-8

ORIGINAL PAPER

Stability enhancement of PSS-UPFC installed power system by support vector regression

Mohammad Shoaib Shahriar[1] · **Md Shafiullah**[1] · **Md Juel Rana**[1]

Received: 1 September 2016 / Accepted: 21 August 2017 / Published online: 4 September 2017

Abstract Ensuring the transient stability of the power system networks is one of the prime challenges in the highly interconnected power systems. Though the low-frequency oscillations are not very harmful initially, failure to damping out may lead the system to go out of synchronism. The employment of flexible AC transmission systems (FACTS) devices may suppress these oscillations effectively in addition to the enhancement of power transfer capability. Among many FACTS devices, unified power flow controller (UPFC) is one of the most sophisticated ones. Tuning the parameters of power system stabilizer (PSS) coordinated with UPFC for a stable system is a multi-objective optimization problem. This paper aims to optimize the parameters of power system stabilizer (PSS) of power network incorporating UPFC using support vector regression (SVR) in real time to damp out the small signal oscillations hence to enhance the transient stability. System eigenvalues obtained from SVR tuned UPFC coordinated PSS and the fixed gain conventional PSS are compared to investigate the efficacy of the proposed technique for different loading conditions. Besides, time domain simulation comparison proves the superiority of the proposed technique over the conventional one. Furthermore, the statistical performance measures for training and testing datasets provide confidence on the developed SVR model.

Keywords Support vector regression (SVR) · Flexible AC transmission systems (FACTS) · Eigenvalues · Low-frequency oscillations · Power system stability · Power system stabilizer (PSS) · Unified power flow controller (UPFC)

✉ Md Shafiullah
shafiullah@kfupm.edu.sa

[1] Department of Electrical Engineering, King Fahd University of Petroleum and Minerals, Dhahran, Kingdom of Saudi Arabia

List of symbols

δ	Rotor angle
ω	Rotor speed
ω_b	Synchronous speed
x_d, x'_d	Synchronous and sub-transient armature reactances
x_q	Quadrature axis synchronous reactance
v_d, v_q	d–q axes generator terminal voltages
id, iq	d–q axes generator armature current
v_t	Generator terminal voltage
V_{dc}	DC-link capacitor voltage
C_{dc}	Capacitance (capacitive reactance) of DC-link capacitor
i_E, i_B	Current in the shunt (exciting) and series (booster) transformer
m_E, δ_E	Modulation index and angle of shunt (excitation) converter
m_B, δ_B	Modulation index and angle of series (boosting) converter
x_E, x_B	Reactance of excitation and boosting transformer
x_{tE}	Reactance of the transformer on the generator side
X_{BV}	Reactance in the bus side
P_m, P_e	Input and output power of generator
M	Inertia constant
H, D	Inertia constant and damping coefficient of generator
K_A, T_A	Gain and time constant of exciter and regulator

E_{fd}	Generator field voltage
E'_q	Internal voltage of generator
V_{ref}	Reference bus voltage
Vb	Infinite Bus voltage
U_{PSS}	Control signal of PSS
σ	Eigenvalue's real part
ζ	Damping ratio of mth eigenvalue
T_1, T_2, T_3, T_4	Time constants
K	Controller gain

1 Introduction

Nowadays most of the power system networks are operating almost at their stability limit as the expansion of the systems required to fulfill the increasing demands are not met for most of the cases due to the constraint of limited resources and environmental factors. The power systems which are interconnected through weak tie lines give rise to poorly damped low-frequency oscillations those ranges from 0.1 to 3 Hz [1]. If adequate damping is not provided immediately after their commencement these low-frequency oscillations keep increasing, eventually causing the system to reach out of synchronism. To solve this problem, the control of generator excitation employing automatic voltage regulator (AVR) is one of the solutions to damp out these low-frequency oscillations. But it has the drawback of creating low-frequency oscillations by decreasing rotor damping torque [2]. Consequently, power system stabilizers (PSS) are being used extensively in order to enhance power system stability against low-frequency oscillations [3] but it may fail to suppress the severe disturbances like three phase fault and may affect the voltage profile as well [4].

On the contrary, the application of flexible alternating current (AC) transmission systems (FACTS) has become prevalent with the advancement of power electronics. The capability of very fast power electronic-based control action has made the FACTS devices a strong candidate for improvement in power system damping in addition to improving power transfer capability [3,5–7]. FACTS devices enhance the system stability by controlling the dynamic states of system parameters which include voltage, current, series and shunt impedance, phase angle, and damping of low-frequency oscillations [8]. Applications of FACTS devices have been reported for various control objectives including optimal power flow (OPF) [9], voltage stability [10], damping inter-area low-frequency oscillations [11]. Prominent series structured controllers include thyristor controlled series compensator (TCSC), static synchronous series compensator (SSSC), the thyristor controlled series reactor (TCSR) etc. Among the shunt controllers static VAR compensator (SVC), static synchronous compensators (STATCOM) and the thyristor controlled reactor (TCR) are widely used. The unified power flow controller (UPFC) is the combined unit which takes advantages of independent series and shunt controllers [12].

UPFC is the most popular and promising second-generation FACTS device and capable of improving transient stability, providing voltage support, reducing power loss, controlling the power transfer among transmission lines and improving damping of low-frequency oscillations [13]. Using a power flow controller, supplementary damping controller and a DC voltage regulator, UPFC does its works. In order to guarantee system stability during disturbances, it is required to maintain proper coordination between UPFC and PSS. A great number of researches have been reported for the coordination among PSS and FACTS devices [14–16]. Different artificial intelligence (AI) techniques were being employed in power system industries in order to solve many complex problems as well as optimizing the parameters of PSS coordinated with FACTS employing backtracking search algorithm (BSA) [16], genetic algorithm(GA) [17], differential evolution (DE) [18], ant colony optimization (ACO) [19], particle swarm optimization (PSO) [20] to improve the power system stability by damping out the small signal oscillations. However, most of these techniques work in the offline mode as these required a very long time to get the optimized parameters for different operating conditions. To estimate the parameters of PSS coordinated with FACTS devices different machine learning techniques, for instance, artificial neural networks, support vector regressions can be employed effectively.

Support vector machines (SVM) can efficiently and effectively solve the multidimensional, nonlinear and complex function estimation problems. Vapnik [21] was the first to introduce it. SVM's are now widely used for both classification and regression problems and the machines dedicated to regression problems are renamed as support vector regression (SVR). Power system industry is also employing these machine to solve many complex problems including stability forecasting and prediction [22], fault location [23], assessment of voltage instability [24]. Although artificial neural network can be used for solving the multidimensional optimization problem, sometimes it suffers from rule obscureness and local convergence [25].

As mentioned earlier, the PSS parameters coordinated with UPFC need be optimized in real-time fashion as the loading conditions of electric networks change continually. The trained SVR model can optimize PSS settings within very short period of time (within two cycles of power system) for any loading condition. The faster computational speed and higher accuracy make the proposed SVR approach suitable for online parameter estimation of PSS coordinated with UPFC. Therefore, this paper contributes to the development of an SVR-based technique for the tuning of optimal parameter setting of PSS connected with UPFC in a single

machine infinite bus (SMIB) electric network. In this paper, the performance of the SVR algorithm is evaluated to estimate the parameters of PSS coordinated with UPFC in real time depending on varying operating conditions to enhance the stability of power system.

The rest of the paper is organized as follows: Sect. 2 presents the detail mathematical model of the system as well as the PSS-UPFC-based control architecture. Optimization problem formulation and data generation strategy have been presented in Sect. 3. Section 4 describes details of support vector regression technique used for problem-solving. Simulation results have been shown and discussed in Sect. 5 and finally, the conclusion is drawn in Sect. 6.

2 Power system dynamic model

2.1 Power system model

A single machine infinite bus (SMIB) system equipped with UPFC has been considered [14] as shown in Fig. 1 where a generator is connected to an infinite bus through the transmission line. UPFC is connected to the power system via excitation transformer (ET) and boosting transformer (BT).Two voltage source converters (VSCs), namely VSC-B and VSC-E are connected through a DC-link common capacitor.

This arrangement works as an ideal bi-directional AC-to-AC power converter. VSC-B is connected in series with the line through boosting transformer and does the work of injecting voltage of variable magnitude. Thus, the output voltage from VSC-B is seen as synchronous AC voltage source. On the other hand, the main task of VSC-E is to supply or absorb the real power which is demanded by VSC-B at the common dc-link in order to support the real power exchange resulting from the series voltage injection. It can also absorb or generate controllable reactive power, if needed, providing the line an independent shunt reactive compensation.

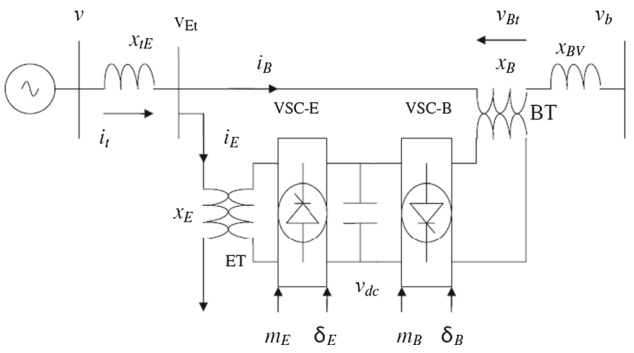

Fig. 1 SMIB system equipped with UPFC [20]

There are four input control parameters of the UPFC which are given by m_E, m_B, δ_E and δ_B. Amplitude modulation ratio plays a key role in all power electronics devices which actually reflects the ratio between modulation amplitude and peak amplitude of the given signal to FACTS devices.

The nonlinear model of SMIB can be represented by the following three differential equations (1)–(3) [26]:

$$\dot{\delta} = \omega_b(\omega - 1) \tag{1}$$

$$\dot{\omega} = \frac{1}{2H}[P_m - D(\omega - 1) - P_e] \tag{2}$$

$$\dot{E}'_q = \frac{1}{T'_{do}}\left[E_{fd} - (x_d - x'_d)i_d - E'_q\right] \tag{3}$$

Terminal voltage (v_t) and output electrical power (P_e) can be written in terms of the direct axis and quadrature axis voltage and current as given below:

$$P_e = v_d i_d + v_q i_q \tag{4}$$

$$v_t = \sqrt{\left(v_d^2 + v_q^2\right)} \tag{5}$$

v_d and v_q can be expressed as the following:

$$v_d = x_q i_q,$$
$$v_q = E_q{}' - x_d{}' i_d,$$
$$i_q = i_{Eq} + i_{Bq}, i_d = i_{Ed} + i_{Bd}$$

Taking the d–q axis, four current quantities $i_{Ed}, i_{Eq}, i_{Bd}, i_{Bq}$ could be found.

2.2 Exciter and power system stabilizer (PSS)

Institute of Electrical and Electronics Engineers (IEEE) permits some of the standard-type excitation systems. The one used for the proposed system model is shown in Fig. 2. An AVR has been used to provide excitation to the system. The Power System Stabilizer (PSS) is the widely used

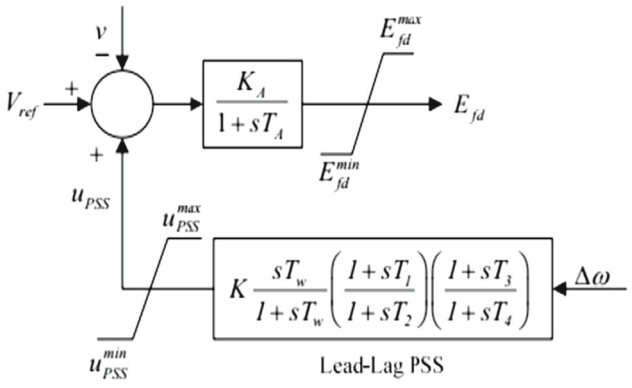

Fig. 2 Block diagram of the excitation system [16]

lead–lag controller which contains a lead–lag block along with a limiter. PSS also includes a washout filter to suppress the steady-state quantity of the input signal. The output of the PSS is a supplementary stabilizing control signal (U_{PSS}) which is found when a change in angular speed ($\Delta\omega$) is given as the input in lead–lag compensator.

This excitation system can be represented by the state equation:

$$\Delta\dot{E}_{fd} = K_A((V_{\mathrm{ref}} - v_t + U_{\mathrm{pss}}) - E_{fd})\frac{1}{T_A} \tag{6}$$

2.3 The dynamic model of the UPFC

The UPFC model has been obtained after park transformation and neglecting the resistances as well as the transients of the Excitation and Boosting transformers [27].

$$\begin{aligned}\dot{v}_{dc} = {} & \frac{3m_E}{4C_{dc}}(\cos\delta_E i_{Ed} + \sin\delta_E i_{Eq}) \\ & + \frac{3m_B}{4C_{dc}}(\cos\delta_B i_{Bd} + \sin\delta_B i_{Bq})\end{aligned} \tag{7}$$

The currents of excitation and boosting transformers (i_{Ed}, i_{Eq}, i_{Bd}, i_{Bq}) in terms of other different parameters can be represented as follows:

$$\begin{aligned}i_{Ed} = {} & \frac{x_{BB}}{x_{d\sum}}E_q{}' - \frac{m_E\sin\delta_E v_{dc}x_{Bd}}{2x_{d\sum}} \\ & + \frac{x_{dE}}{x_{d\sum}}\left(v_b\cos\delta + \frac{m_B\sin\delta_B v_{dc}}{2}\right) \\ i_{Eq} = {} & \frac{m_E\cos\delta_E v_{dc}x_{Bq}}{2x_{q\sum}} \\ & - \frac{x_{qE}}{x_{q\sum}}\left(v_b\sin\delta + \frac{m_B\sin\delta_B v_{dc}}{2}\right) \\ i_{Bd} = {} & \frac{x_E}{x_{d\sum}}E_q{}' + \frac{m_E\sin\delta_E v_{dc}x_{dE}}{2x_{d\sum}} \\ & - \frac{x_{dt}}{x_{d\sum}}\left(v_b\cos\delta + \frac{m_B\sin\delta_B v_{dc}}{2}\right) \\ i_{Bq} = {} & -\frac{m_E\cos\delta_E v_{dc}x_{qE}}{2x_{q\sum}} \\ & + \frac{x_{qt}}{x_{q\sum}}\left(v_b\sin\delta + \frac{m_B\cos\delta_B v_{dc}}{2}\right)\end{aligned}$$

where

$$\begin{aligned}x_{qt} &= x_q + x_{tE} + x_E, x_{qE} = x_q + x_{tE}, \\ x_{dt} &= x_d' + x_{tE} + x_E, x_{dE} \\ &= x_d' + x_{tE}, x_{BB} = x_B + x_{BV}, \\ x_{q\sum} &= x_{qt}.x_{BB} + x_e.x_{qE} \\ &= (x_q + x_{tE} + x_E)(x_B + x_{BV}) + x_e(x_q + x_{tE}), \\ x_{Bq} &= x_{BB} + x_{qE} = x_B + x_{BV} + x_q + x_{tE}, \\ x_{d\sum} &= x_{dt}x_{BB} + x_E x_{dE} \\ &= (x_d' + x_{tE} + x_E)(x_B + x_{BV}) + x_E(x_d' + x_{tE}), \\ x_{Bd} &= x_{BB} + x_{dE} = x_B + x_{BV} + x_d' + x_{tE}\end{aligned}$$

The constant values of reactance used for the modeling purpose are provided in appendix section.

2.4 UPFC coordinated PSS (damping controller)

The damping controller produces an electrical torque that is in phase with speed deviation using phase compensation technique. The damping torque is controlled by the four control parameters of UPFC such as δ_B, m_B, m_E and δ_E. The lead–lag damping controllers equipped with UPFC are of the structure as presented in Fig. 3 [28], where the output of the UPFC is the control signal input (u). The value of control signal(u) can be any one of the signals mE, mB or δB.

The DC voltage is regulated by changing the voltage phase angle (δ_E) of the excitation transformer (ET). The modulated value of δ_E is obtained from the controller shown in Fig. 4 where PI controller acts as a voltage regulator.

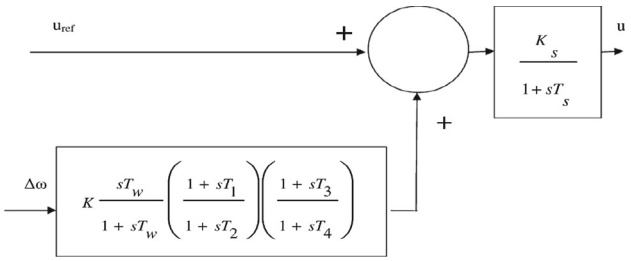

Fig. 3 Lead–lag controller-based UPFC [28]

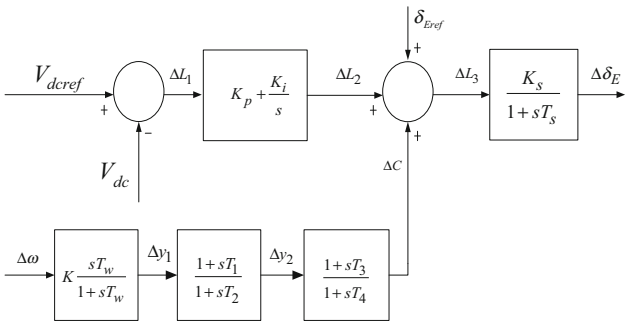

Fig. 4 Lead–lag controller and DC voltage regulator with UPFC

2.5 Linearized model

For controller design, the linear model of the system has been considered. The nonlinear dynamic equations presented in (1)–(7) can be linearized by taking a small variation of the parameters around a given operating point and the linearized system can be written in state-space form as [27]:

$$\dot{X} = A\Delta X + B\Delta U \tag{8}$$

Here, $\boldsymbol{A}$ and $\boldsymbol{B}$ are the constant matrices of the system which is directly dependent upon the operating state of the system. The full forms of the matrices of equations 8 are presented in "Appendix C".

The following state equations can be derived from the block diagram of Fig. 4 which will be further added to state Eq. (8) at the time of finding out the closed loop state matrix A_c.

$$\Delta\dot{y}_1 = [K\Delta\dot{\omega}T_w - \Delta y_1]\frac{1}{T_w} \tag{9}$$

$$\Delta\dot{y}_2 = [\Delta y_1 + \Delta\dot{y}_1 T_1 - \Delta y_2]\frac{1}{T_2} \tag{10}$$

$$\Delta\dot{c} = \left[-\Delta c + \Delta\dot{\delta}_E T_3 + \Delta y_2\right]\frac{1}{T_4} \tag{11}$$

$$\Delta\dot{L}_2 = K_p\Delta\dot{L}_1 + K_i\Delta L_1 \tag{12}$$

$$\Delta\dot{\delta}_E = [K_3\Delta L_3 - \Delta\delta_E]\frac{1}{T_s} \tag{13}$$

The Eigenvalues of the state matrix A_c will represent the modes of the system after being subjected to any small disturbance. The negative real part will ensure the stable condition of the system. For the case of an unstable situation with positive real part of any of the Eigenvalues, the system can be brought into the stable state again by using the output or the state feedback controller. In that case, the state equation will be modified in the following form containing closed loop state matrix A_c:

$$\dot{X} = A_c X \tag{14}$$

Eventually, the dimension of the matrix $\mathbf{A}_c$ will be 9 by 9 which will provide nine eigenvalues and the details about this matrix can be found in [28,29]. It is worth mentioning that in this paper the PI controller block of Fig. 4 is kept deactivated throughout the simulation period and the considered state variables of equation (14) are $\Delta\delta, \Delta\omega, \Delta E'_q, \Delta E_{fd}, \Delta V_{dc}, \Delta C, \Delta y_1, \Delta y_2,$ and $\Delta\delta_E$. However, the $\mathbf{A}_c$ matrix generated eigenvalues can be shifted to the negative part of the complex plane ensuring the desirable performance of the system through the proper selection of UPFC coordinated PSS parameters.

3 Optimization problem formulation

In the optimization problem, two objective functions are used which are basically based on Eigenvalues of the states. First one focuses on improving the damping factor of the system and the other one will ensure the satisfactory value of damping ratio. The combination of these two objective functions, J_1 and J_2 will form the multi-objective function J which can be represented as follows [30]:

$$J = J_1 + \alpha J_2 \tag{15}$$

$$J = \sum_{\sigma_{mn}\geq\sigma_0}(\sigma_0 - \sigma_{mn})^2 + \alpha\sum_{\zeta_m\geq\zeta_0}(\zeta_0 - \zeta_m)^2 \tag{16}$$

where m represents the Eigenvalue index of the system and n is the index of system operating conditions. σ_{mn} is the Eigenvalue's real part upon which relative stability of the system mostly depends. The damping ratio is represented by ζ. Two objective functions are combined by a weighting factor α and the value has been chosen 10 in this work.

The graphical representation of each of the objective functions is presented in Fig. 5. Figure 5a reflects that the closed loop Eigenvalues will be forced toward the negative half plane and will be placed in the indicated dashed region if the objective function J_1 has been taken only. In the same way, Fig. 5b shows that the maximum overshoot of the Eigenval-

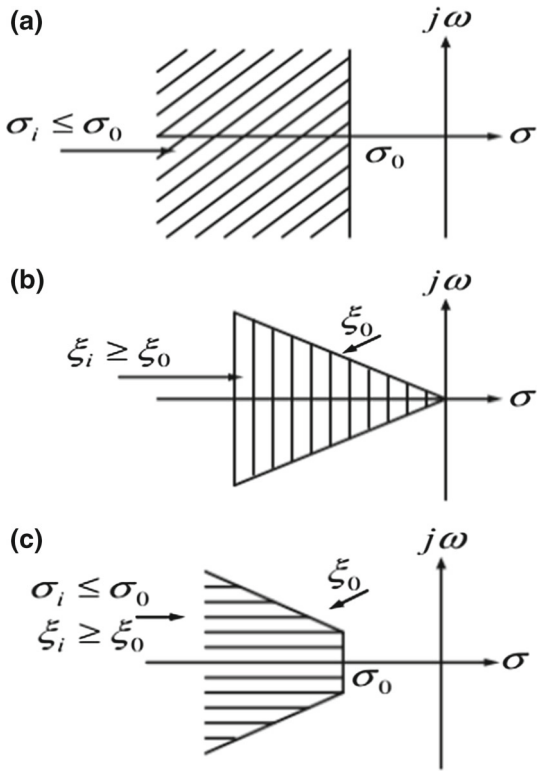

Fig. 5 Eigenvalue locations for corresponding objective function [30]

ues is controlled by choosing only J_2 as the objective function and will limit it within the particular dashed region. When the objective function J is optimized, because of the effect of J_1 and J_2, the generated Eigenvalues of the system will be confined inside the D-shaped shaded region as presented in Fig. 5c.

This will ensure the stability of the system by meeting the requirements of the required damping factor and ratio for a stable system. Real parts of the Eigenvalues will be forced to be placed in the negative half plane within a specific overshoot range. So, the optimization problem can be stated as:

Minimize J

Subject to

$$K^{\min} \leq K \leq K^{\max}$$
$$T_1^{\min} \leq T_1 \leq T_1^{\max}$$
$$T_2^{\min} \leq T_2 \leq T_2^{\max}$$
$$T_3^{\min} \leq T_3 \leq T_3^{\max}$$
$$T_4^{\min} \leq T_4 \leq T_4^{\max}$$

To ensure the stability of the system during transients in the power system the optimum value of the controller parameters must be determined aiming to optimize objective function J. In this work objective function optimization translates into maximizing the minimum value of the damping ratio subject to some inequality constraints. The constraints for this optimization problem are lower and upper limit of time constants $(T_1 - T_4)$ and controller gain (K).

Subject to the same five constraints stated above to keep the controller gain and four-time constants of lead–lag compensators within the desired range. The optimum parameters of the controller are predicted online employing trained and tested SVR.

4 Proposed methodology

4.1 Data generation

The loading conditions comprising of the per unit values of three variables of synchronous machine, namely real power (P_e), reactive power (Q_e) and terminal voltage (V_t), have been used for data generation and the ranges of these variables are:

$$0.40 \leq P_e \leq 1.10$$
$$-0.30 \leq Q_e \leq 0.30$$
$$0.90 \leq V_t \leq 1.10$$

With a view to training and testing the SVR, a set of one thousand optimal parameters $(K\&T_1)$ for PSS coordinated with UPFC were generated for different loading conditions employing backtracking search algorithm (BSA) by setting some constant values to T_2, T_3, and T_4 as the parameters $T_1 - T_4$ are related to each other. The main operators of BSA are initialization, selection-I, mutation, crossover, and selection-II. Though BSA shares the similar name for the operators with genetic algorithm (GA), but the mutation and crossover operations of BSA are completely different from GA. Additionally, the boundary control mechanism is different from GA or other evolutionary techniques. The details about BSA can be found in [31–34]. Real power (P_e), reactive power (Q_e) and terminal voltage (V_t) representing the loading conditions were taken as the inputs (independent variables) whereas BSA tuned optimal PSS parameters $(K\&T_1)$ coordinated with UPFC were taken as the targets (dependent variables) to the SVR. From the prepared dataset 70% of data have been selected randomly for training and rest of them were selected for testing the SVR model.

4.2 Support vector regression model

The methodology of SVR follows Structural Risk Minimization (SRM) principle which tries to minimize the upper bound on the expected risk. This has been found better than empirical risk minimization process, implied by conventional neural networks to minimize the error of the training data [35]. The training data of support vector regression (SVR) is mapped in a high-dimensional feature space which is also known as Hilbert space and turns the nonlinear regression function into a linear one by proper mapping. Because of the following of SVR, it can perform well even with the fewer number of data samples.

Formation of data set is the first step for training model followed by testing phase. Let us consider $\{(x_1, y_1), \ldots, (x_m, y_m)\}$ as a set of training data where each of the x_i represents m-dimensional input space of the sample and y_i is the corresponding outputs (target values) for $i = 1, 2, \ldots, m$ and m represents the size of the training data. If the fitting function is denoted by $f(x)$, then the SVR can reach the target y for the corresponding testing sample x through $f(x)$ after the training will be done.

With these training data, SVR forms the mapping function (estimation function) like [36]:

$$f(x) = w \cdot \phi(x) + b \tag{17}$$

Here ω is the weight vector, b represents the bias and $\phi(x)$ is the high-dimensional space mapped from the input space x_i. In order to get the estimated value of ω and b, minimizing the following regression risk function is required:

$$R_{reg}(f) = C\sum_{i=0}^{m}\psi(f(x_i) - y_i) + \frac{1}{2}\|w\|^2 \tag{18}$$

where $\psi(.)$ the cost function and C is a particular constant. Substituting the value of the weight vector

$$w = \sum_{i=1}^{m}(a_i - a_i^*)\phi(x_i)$$

in Eq. (17) will give us the modified generic equation:

$$\begin{aligned} f(x) &= \sum_{i=1}^{m}(a_i - a_i^*)(\phi(x_i)\cdot\phi(x)) + b \\ &= \sum_{i=1}^{m}(a_i - a_i^*)k(x_i, x) + b \end{aligned} \tag{19}$$

The dot product of Eq. (19) can is replaced by $k(x_i, x)$ which is known as Kernel function that helps to use the dot product in low- dimensional space data input without knowing $\phi(x)$. Besides, ε-insensitive loss function must have to be satisfied in order to ensure robustness of the regression result as well as to ensure the sparsity of the solution. The function is as follows [37]:

$$\psi(f(x) - y) = \begin{cases} |f(x) - y| - \varepsilon, & \text{for } |f(x) - y| \geq \varepsilon \\ 0, & \text{otherwise} \end{cases} \tag{20}$$

The problem of regression risk in Eq. 18 and ε-insensitive loss function of Eq. 20 can be solved using quadratic optimization problem and can be represented as:

$$\begin{aligned} &\frac{1}{2}\sum_{i,j=1}^{m}(a_i^* - a_i)(a_j^* - a_j)k(x_i, x_j) \\ &-\sum_{i=1}^{m}a_i^*(y_i - \varepsilon) - a_i^(y_i + \varepsilon) \end{aligned}$$

Subject to

$$\sum_{i=1}^{m}a_i - a_i^* = 0, a_i, a_i^* \in [0, C]$$

Here, in the optimization problem formulation presented above, a_i and a_i^* are the Lagrange multipliers which represent the solution of the quadratic function. These help the prediction to reach the targeted values y_i. Nonzero values of these Lagrange are known as support vectors and they are actually responsible for forecasting the regression line properly. It happens only when the condition $|f(x) - y| \geq \varepsilon$ is satisfied. Thus, the value of w can be obtained.

In order to get the value of constant b, well-known KKT (Karush Kuhn Tucker) condition needs to be applied which says that the multiplication of constraints and the Lagrange multipliers will be zero.

$$\begin{aligned} &a_i(\varepsilon + \xi_i - y_i + (w, x_i) + b) = 0 \\ &a_i^*(\varepsilon + \xi_i^* + y_i - (w, x_i) - b) = 0 \\ &(C - a_i)\xi_i = 0 \\ &(C - a_i^*)\xi_i^* = 0 \end{aligned}$$

Here, ξ_i and ξ_i^* are the slack variables which are used to calculate the errors ε outside the boundary. Bias constant b could be found from the above equations as:

$$\begin{aligned} &a_i = a_i^* = \xi_i^* = 0 \\ &b = y_i - (w, x_i) - \varepsilon for a_i \in (0, C) \\ &b = y_i - (w, x_i) + \varepsilon for a_i^* \in (0, C) \end{aligned}$$

Thus the SVR will be ready to search for the target for some provided input dataset without even knowing the transformation. The penalty C, imposed for estimation error needs to be examined so as the value of ε which will decide the specific data to be ignored while doing regression.

In this paper, the proposed SVR model optimizes two key parameters of the PSS coordinated with UPFC, namely gain (K) and time constant (T_1).It is worth mentioning that the key issue in designing PSS coordinated with UPFC is to ensure appropriate phase lead which can be achieved by keeping T_2, T_3, and T_4 as constants and optimizing K and T_1. The complete flow diagram of the work procedure is shown in "Appendix D".

5 Simulation results and discussions

5.1 Performance of support vector regression

In this paper, three variables of synchronous machine, namely real power (P_e), reactive power (Q_e) and terminal voltage (V_t) were taken as the inputs and corresponding optimized PSS parameters $(K\&T_1)$ with UPFC were taken as outputs. The number of training and testing data, as well as the required constant parameters for SVR, are presented in Table 1 which has been used in this work.

With a view to examining the performance of the proposed SVR in estimating PSS parameters with UPFC, mean squared error (MSE), root mean squared error (RMSE), mean absolute percentage error (MAPE) and the coefficient of determination (R^2) were determined for each parameter. Mathematical formulas used for the error measures are presented in "Appendix A". The smaller values of MSE, RMSE and MAPE refer the strength of the proposed method.

Table 1 Parameter used for SVR model

C	500
λ	8.938×10^{-3}
$\in$	5.000×10^{-6}
Kernel option	300
Kernel type	Gaussian
Training data	934
Testing data	234
Inputs	Real power (P_e), reactive power (Q_e) and terminal voltage (V_t)
Outputs	PSS parameters (K & T_1)

Table 2 Recorded statistical measures of SVR model

Parameter		RMSE	MAPE	R^2
K	For training	2.4327	0.064716	0.99121
	For testing	2.2344	0.064134	0.99250
T_1	For training	0.0058134	0.0042699	0.99997
	For testing	0.0059786	0.0043896	0.99996

Additionally, the value '1' for R^2 indicates a perfect match between actual and predicted values whereas the value '0' indicates no match at all. The statistical measures for the proposed technique are tabulated in Table 2, where smaller values of MSE, RMSE, and MAPE give confidence over developed technique. Furthermore, the table also shows the values of R^2 are very close to 1.00 for all the parameters which indicate a very good match of between the BSA optimized generated data and SVR estimated values.

5.2 Required time to estimate UPFC coordinated PSS parameters

The simulation was carried out in MATLAB environment and in an Intel Xeon (3.06 GHz -2 Processors, 24 GB RAM) workstation computer. As the SVR takes different times for training and testing purposes for each run, the average training and testing times for one hundred runs were 58.0938 and 0.0169 s, respectively. Furthermore, the average time required for calculation of initial values and determination of optimal parameters for one hundred loading conditions were also recorded and times were 0.0025 and 0.0021 s, respectively. So the overall time required for SVR to estimate optimized values of UPFC is 0.0046 s which is less than 2 cycles of a 60 Hz electric system. As the proposed technique can stabilize a disturbed network in less than two cycles of time, the technique can be implemented in the real-time application.

Table 3 Comparison of Eigenvalues for nominal loading

($P_e = 0.98$ pu, $Q_e = 0.16$ pu and $V_t = 1.00$ pu)	
Fixed gain PSS with UPFC	SVR optimized PSS with UPFC
−994.470	−981.117
−110.704	−126.412
−86.4973	−80.4168
−6.69483	−1.09448
−0.2055099	−0.19785
−0.4187228 ± j4.609576	−4.463426 ± j3.875731
−0.6764214 ± j0.3198909	−1.298876 ± j0.6286555

Table 4 Comparison of Eigenvalues for light loading

$P_e = 0.60$ pu, $Q_e = 0.01$ pu and $V_t = 0.98$ pu	
Fixed gain PSS with UPFC	SVR optimized PSS with UPFC
−993.511	−977.669
−110.031	−127.012
−87.5622	−83.4700
−6.59300	−1.16172
−0.39972	−0.391011
−0.6145031 ± j3.968494	−4.114752 ± j2.871297
−0.7181086 ± j0.2952085	−1.414695 ± j0.2599829

Table 5 Comparison of Eigenvalues for heavy loading

$P_e = 1.30$ pu, $Q_e = 0.40$ pu and $V_t = 1.06$ pu	
Fixed gain PSS with UPFC	SVR optimized PSS with UPFC
−991.096	−969.179
−112.996	−135.357
−87.0478	−82.6872
−7.26873	−2.59196
−0.14723	−0.1434418
−0.4268946 ± j4.800489	−4.346762 ± j2.995125
−0.6766701 ± j0.2739384	−1.055703 ± j0.1860413

5.3 Eigenvalues and minimum damping ratio comparison

The SMIB with UPFC was simulated for three loading conditions, namely nominal, light and heavy loading conditions. System stability can be determined through analysis of eigenvalues. Eigenvalues for three different loading conditions, namely nominal, light and heavy loading conditions for both SVR optimized PSS with UPFC and fixed gain conventional PSS with UPFC are tabulated in Tables 3, 4 and 5. The tables show all the eigenvalues have negative real part means the systems are stable but the fixed gain PSS with UPFC needs more time to settle the disturbance down than the optimized

Table 6 Damping ratio comparison for different loading conditions

Loading conditions				Minimum Damping ratio		
	Pe(pu)	*Qe*(pu)	*Vt*(pu)	Fixed gain PSS with UPFC	BSA optimized PSS with UPFC	SVR optimized PSS with UPFC
Nominal	0.98	−0.16	1.00	0.0905	0.7428	0.7551
Light	0.60	0.01	0.98	0.1530	0.8197	0.8201
Heavy	1.30	0.40	1.06	0.0886	0.8322	0.8234

one as its complex eigenvalues are relatively close to the imaginary (jω) axis.

Obtained minimum damping ratios for fixed gain conventional PSS with UPFC, SVR optimized PSS with UPFC and BSA optimized PSS with UPFC (offline) are tabulated in Table 6 for different loading conditions. It is clear from the table that optimized parameters have better values than conventional fixed gain one which signals that better damping will be achieved with optimized PSS with UPFC. However, as BSA-based optimization is carried out is offline, it cannot be applied in real-time application.

Both minimum damping ratios and eigenvalues comparisons clearly signal the better performance of SVR optimized PSS with UPFC over conventional fixed gain one in settling down the small frequency oscillations after being subjected to any disturbances in real-time operation of power system network.

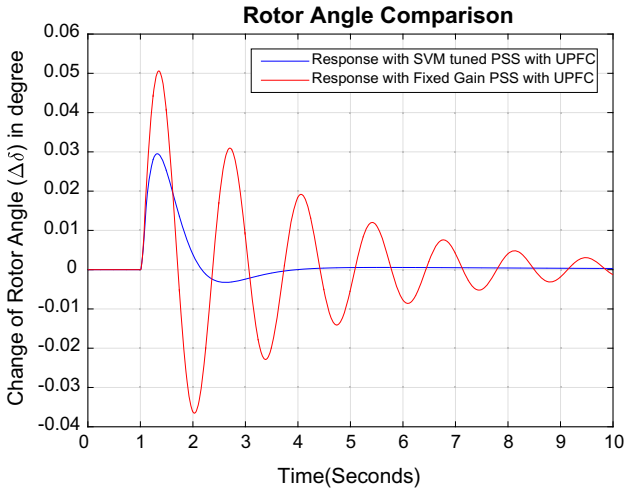

Fig. 6 Response of $\Delta\delta$ for SVR tuned and fixed gain power system stabilizer coordinated with UPFC

5.4 Time domain simulation results with disturbance

The performance of SVR optimized PSS with UPFC for damping small frequency oscillations in case of disturbance has been compared with conventional one having fixed gain. To simulate the disturbance a 10% pulse input of mechanical torque has been applied at 1.0 s for 4 cycles and corresponding system responses have been observed. Both conventional and SVR optimized PSS with UPFC stabilize the power system network after being subjected to mechanical disturbance. However, SVR optimized PSS with UPFC exhibits faster response compared to the conventional one as shown in Figs. 6, 7 and 8 for nominal loading condition.

Figures 6, 7 and 8 reflect the transient behavior of three of the system states $\Delta\delta$, $\Delta\omega$, and ΔV_{dc}, respectively. When the PSS parameters are selected randomly for fixed gain PSS with UPFC, the response of the states take very long time to reach the stable state. In each of the three figures below, it is reflected that the system couldn't reach the stable stage even within the 10 s time span provided in the simulation. Whereas oscillations in $\Delta\omega$ states become stable in around 2.7 s (Fig. 7) and $\Delta\delta$ in 4 s (Fig. 6) when the control parameters are optimized with proposed SVR optimization.ΔV_{dc} requires a bit higher time than others but still makes the system oscillation-free within around 5 s (Fig. 8). It signifies the effect of using SVR algorithm in the field of power system stability.

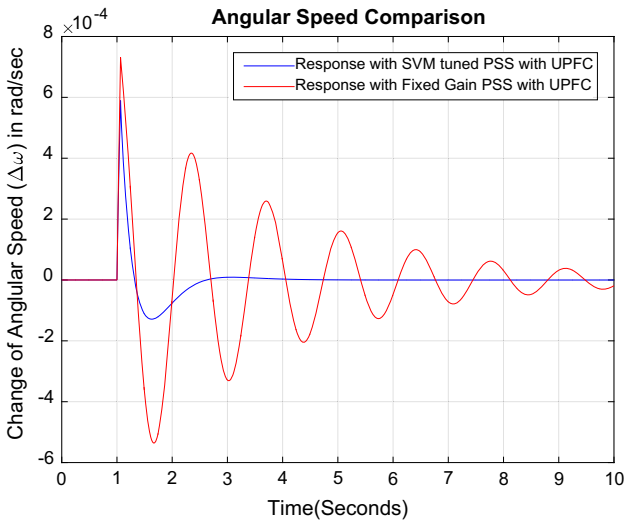

Fig. 7 Response of $\Delta\omega$ for SVR tuned and fixed gain power system stabilizer coordinated with UPFC

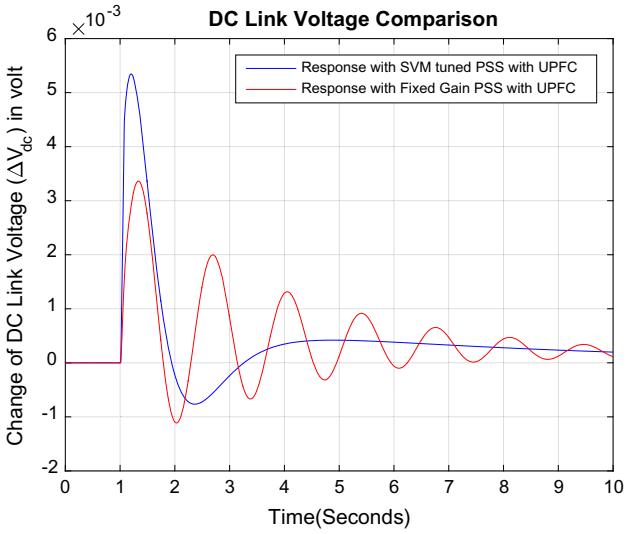

Fig. 8 Response of ΔV_{dc} for SVR tuned and fixed gain power system stabilizer coordinated with UPFC

6 Conclusions

Investigating the real-time performance of UPFC coordinated PSS connected power system subjected to low-frequency oscillations is the main objective of this paper. Support vector regression model estimates the parameters of PSS coordinated with UPFC in real-time fashion. The performance of proposed technique is tested for three different loading conditions. In addition, the obtained results are compared with the fixed gain PSS coordinated with UPFC. From the eigenvalue analysis and time domain representation of system parameters, it is seen that proposed controller outperforms the conventional one in all respect. Furthermore, it is found that the time required for the SVR model to tune the controller parameters is less than two cycles of a 60 Hz power system. Thus, in terms of computational speed and accuracy, the proposed model presents its efficiency as a real-time optimizer and ensures robustness in power system stability enhancement. Besides, satisfactory values of the statistical performance measures for training and testing datasets provide confidence on the proposed SVR model. However, the idea presented in this paper can be further extended for tuning the PSS parameters of a multimachine power system network.

Appendix A

System parameters used are given below:
Generator and transmission line:
M = 8MJ/MVA, D = 0, x_d = 1.0pu, x_q = 0.6pu, T'_{d0} = 5.044s, x'_d = 0.3pu, ω_b = 377rad/s and X_L = 0.1pu
Machine excitation system: $K_A = 100$, $T_A = 0.01s$
Transformer: X_T = 0.1pu, $X_E = 0.1\,pu$, and X_B = 0.1pu
DC-link:
v_{DC} = 2pu and C_{DC} = 1.2pu
parameters (Fixed gain):
UPFC: $\delta_E = 68.113$deg, $\delta_B = 41.12$deg, $m_B = 0.96$, $m_E = 0.7667$
PSS: $K = 15.71$, $T_1 = 0.3$ s, $T_2 = 0.3$ s, $T_3 = 0.39$ s, $T_4 = 0.6623$ s
PSS parameters: $1 \le K \le 50$, $0.01 \le T_1 \le 1.0$

$$\text{Eigenvalue} : \lambda = \sigma + j\omega \tag{A.1}$$

$$\text{DampingRatio} : \zeta = -\frac{\sigma}{\sqrt{\sigma^2 + \omega^2}} \tag{A.2}$$

Appendix B

The performance of the proposed technique was tested with different well-known error measures including mean squared error (MSE), root mean squared error (RMSE), mean absolute percentage error (MAPE) and the coefficient of determination (R^2).

For total n data samples, actual values y_a and predicted values y_p, mathematical formulas for the error measures are presented below:

$$\text{MSE} = \sum_{i=1}^{n} ((y_a)_i - (y_p)_i)^2 \tag{A.3}$$

$$\text{RMSE} = \sqrt{\frac{\sum_{i=1}^{n} ((y_a)_i - (y_p)_i)^2}{n}} \tag{A.4}$$

$$\text{MAPE} = \frac{1}{n} \sum_{i=1}^{n} \left| \frac{(y_a)_i - (y_p)_i}{(y_a)_i} \right| \times 100 \tag{A.5}$$

$$R^2 = 1 - \sum_{i=1}^{n} \frac{((y_a)_i - (y_p)_i)^2}{((y_a)_i - \bar{y}_a)^2} \tag{A.6}$$

where $\bar{y}_a$ is the mean of actual value.

Appendix C

The state vector $\Delta X = [\Delta\delta, \Delta\omega, \Delta E'_q, \Delta E_{fd}, \Delta V_{dc}]^T$
Control vector $\Delta U = [\Delta U_{\text{pss}}, \Delta m_E, \Delta\delta_E, \Delta m_B, \Delta\delta_B]^T$

$$A = \begin{bmatrix} 0 & \omega_b & 0 & 0 & 0 \\ -\frac{K_1}{M} & -\frac{D}{M} & -\frac{K_2}{M} & 0 & -\frac{K_{pd}}{M} \\ -\frac{K_4}{T'_{d0}} & 0 & -\frac{K_3}{T'_{d0}}\frac{1}{T'_{d0}} & -\frac{K_{qd}}{T'_{d0}} & \\ -\frac{K_A K_5}{T_A} & 0 & -\frac{K_A K_6}{T_A} & -\frac{1}{T_A} & -\frac{K_A K_{vd}}{T_A} \\ K_7 & 0 & K_8 & 0 & -K_9 \end{bmatrix}$$

$$B = \begin{bmatrix} 0 & 0 & 0 & 0 & 0 \\ 0 & -\frac{K_{pe}}{M} & -\frac{K_{pde}}{M} & -\frac{K_{pb}}{M} & -\frac{K_{pdb}}{M} \\ 0 & -\frac{K_{qe}}{T'_{d0}} & -\frac{K_{qde}}{T'_{d0}} & \frac{K_{qb}}{T'_{d0}} & -\frac{K_{qdb}}{T'_{d0}} \\ \frac{K_A}{T_A} & -\frac{K_A K_{ve}}{T_A} & -\frac{K_A K_{vde}}{T_A} & -\frac{K_A K_{vb}}{T_A} & -\frac{K_A K_{vdb}}{T_A} \\ 0 & K_{ce} & K_{cde} & K_{cb} & K_{cdb} \end{bmatrix}$$

Appendix D

Stability enhancement method:

The remote terminal unit (RTU) at synchronous generator end measures the real power, reactive power, and terminal voltage continually and based on these values the proposed method estimates the initial conditions and then the PSS parameters with UPFC are optimized through SVR. The following flowchart illustrates the whole online optimization process (Fig. 9).

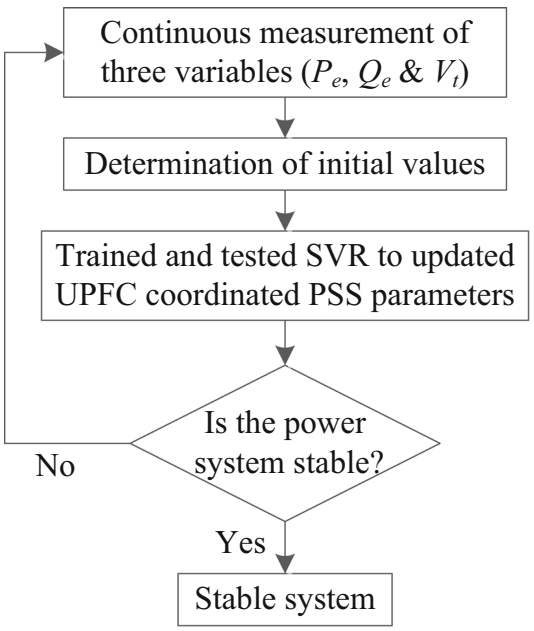

Fig. 9 Flowchart of proposed SVR-based approach

References

1. Kundur P, Balu NJ, Lauby MG (1994) Power system stability and control. McGraw-Hill, New York
2. Sambariya DK, Prasad R (2013) Design of PSS for SMIB system using robust fast output sampling feedback technique. In: 7th International conference on intelligent systems and control (ISCO). IEEE, pp 166–171
3. Larsen E, Swann D (1981) Applying power system stabilizers part I: general concepts. IEEE Trans Power Appar Syst PAS–100(6):3017–3024
4. Abido MA, Al-Awami AT, Abdel-Magid YL (2006) Imultaneous design of damping controllers and internal controllers of a unified power flow controller. In: IEEE power engineering society general meeting. IEEE, p 8
5. Shareef H, Mohamed A, Eslami M (2010) Application of PSS and FACTS devices for intensification of power system stability. Int Rev Electr Eng 5(2):552–570
6. Alam MS, Razzak MA, Shafiullah M, Chowdhury AH (2012) Application of TCSC and SVC in damping oscillations in Bangladesh Power System. In: 7th International conference on electrical and computer engineering. IEEE, pp 571–574
7. Alam MS, Shafiullah M, Hossain MI, Hasan MN (2015) Enhancement of power system damping employing TCSC with genetic algorithm based controller design. In: International conference on electrical engineering and information communication tech. (ICEEICT). IEEE, pp 1–5
8. Siddiqui AS, Khan MT, Iqbal F (2015) Determination of optimal location of TCSC and STATCOM for congestion management in deregulated power system. Int J Syst Assur Eng Manag 8(1):110–117
9. Mukherjee A, Mukherjee V (2016) Solution of optimal power flow with FACTS devices using a novel oppositional krill herd algorithm. Int J Electr Power Energy Syst 78:700–714
10. Inkollu SR, Kota VR (2016) Optimal setting of FACTS devices for voltage stability improvement using PSO adaptive GSA hybrid algorithm. Eng Sci Technol Int J 19:1166–1176
11. Castoldi MF, Sanches DS, Mansour MR, Bretas NG, Ramos RA (2014) A hybrid algorithm to tune power oscillation dampers for FACTS devices in power systems. Control Eng Pract 24:25–32
12. Khan MT, Siddiqui AS (2016) FACTS device control strategy using PMU. Perspect Sci 8:730–732
13. Wartana IM, Agustini NP (2011) Optimal placement of UPFC for maximizing system loadability and minimizing active power losses in system stability margins by NSGA-II. In: Proceedings of the 2011 international conference on electrical engineering and informatics. IEEE, pp 1–6
14. Shafiullah M, Alam MS, Hossain MI, Hasan MN (2014) Transient performance improvement of power system by optimal design of SVC controller employing genetic algorithm. In: 8th International conference on electrical and computer engineering. IEEE, pp 540–543
15. Shahriar MS, Shafiullah M, Asif MA, Hasan MM, Ishaque A (2016) Comparison of invasive weed optimization (IWO) and particle swarm optimization (PSO) in improving power system stability by UPFC controller employing a multi-objective approach. In: 1st International conference on advanced information and communication technology 2016 (ICAICT 2016). Chittagong Independent University, Bangladesh, Chittagong, Bangladesh, pp 1–7
16. Shahriar MS, Shafiullah M, Asif MA, Hasan MM, Rafiuzzaman M (2015) Design of multi-objective UPFC employing backtracking search algorithm for enhancement of power system stability. In: 18th International conference on computer and information technology (ICCIT). IEEE, pp 323–328
17. Hassan LH, Moghavvemi M, Almurib HAF, Muttaqi KM (2013) A coordinated design of PSSs and UPFC-based stabilizer using Genetic Algorithm. In: IEEE industry applications society annual meeting. IEEE, pp 1–9
18. Vanitila R, Sudhakaran M (2012) Differential Evolution algorithm based weighted additive FGA approach for optimal power flow using muti-type FACTS devices. In: International conference on emerging trends in electrical engineering and energy management (ICETEEEM). IEEE, pp 198–204
19. Hamid Z, Musirin I, Othman MM, Khalil MR (2010) Optimum tuning of unified power flow controller via ant colony optimization technique. In: 4th International power engineering and optimization conference (PEOCO). IEEE, pp 170–177

20. Al-Awami AT, Abdel-Magid YL, Abido MA (2007) A particle-swarm-based approach of power system stability enhancement with unified power flow controller. Int J Electr Power Energy Syst 29(3):251–259
21. Vapnik VN (1999) An overview of statistical learning theory. IEEE Trans Neural Netw 10(5):988–999
22. Li DH, Cao YJ (2005) SOFM based support vector regression model for prediction and its application in power system transient stability forecasting. In: 2005 International power engineering conference, vol. 2. pp 765–770
23. Shafiullah M, Ijaz M, Abido MA, Al-Hamouz Z (2017) Optimized support vector machine & wavelet transform for distribution grid fault location. In: 11th IEEE international conference on compatibility, power electronics and power engineering (CPE-POWERENG). IEEE, pp 77–82
24. Abdul Wahab MDNI, Mohamed A (2006) Transient stability assessment of a large actual power system using least squares support vector machine with enhanced feature selection. In: Australasian Universities Power Engineering Conference (AUPEC), pp 1–6
25. Zhang W, Hu W, Min Y, Chen L, Zheng L, Liu X (2015) A novel stability classifier based on reformed support vector machines for online stability assessment. In: IEEE PES Asia-Pacific power and energy engineering conference (APPEEC) 2015. pp 1–5
26. Shayeghi H, Shayanfar H, Jalilzadeh S (2009) Simultaneous coordinated designing of UPFC and PSS output feedback controllers using PSO. J Electr 60:177–184
27. Ahmed MA, Shahriar MdS, Ullah MS (2012) Design and analysis of a model predictive unified power flow controller (MPUPFC) for power system stability assessment. Int J Electr Comput Sci 2(4):32–37
28. Shoaib Shahriar MS (2012) Model predictive unified power flow controller (MPUPFC): performance analysis of an MPUPFC for power system stability assessment. LAP LAMBERT Academic Publishing, Germany
29. Shayeghi H, Shayanfar H, Jalilzadeh S (2009) Simultaneous coordinated designing of UPFC and PSS output feedback controllers using PSO. J Electr Eng 60(4):177–184
30. Ajami A, Armaghan M (2010) Application of multi-objective PSO algorithm for power system stability enhancement by means of SSSC. Int J Comput Electr Eng 2(5):838–845
31. Shafiullah M, Abido MA, Coelho LS (2015) Design of robust PSS in multimachine power systems using backtracking search algorithm. In: 18th Proceedings of the Conference on international conference on intelligent system application to power systems (ISAP), pp 1–6
32. Shafiullah M, Rana MJ, Alam MS, Uddin MA (2016) Optimal placement of phasor measurement units for transmission grid observability. In: International conference on innovations in science, engineering and technology (ICISET). IEEE, Chittagong, Bangladesh, pp 1–4
33. Civicioglu P (2013) Backtracking search optimization algorithm for numerical optimization problems. Appl Math Comput 219(15):8121–8144
34. Shafiullah M, Rana MJ, Coelho LS, Abido MA, Al-Subhi A (2017) Designing lead-lag PSS employing backtracking search algorithm to improve power system damping. In: The 9th IEEE GCC conference & exhibition, Manama, Bahrain, pp 1–6
35. Razzak SA, Hossain MI, Rahman SM, Hossain MM (2014) Application of support vector machine modeling on phase distribution in the riser of an LSCFB reactor. Int J Chem React Eng 12:123–134
36. Ramli MAM, Twaha S, Al-Turki YA (2015) Investigating the performance of support vector machine and artificial neural networks in predicting solar radiation on a tilted surface: Saudi Arabia case study. Energy Convers Manag 105:442–452
37. Zhao X, Wang P, Li B (2012) Soft sensor modeling for the efficiency of steam turbine last stage group using support vector machine regression. In: 2012 Second International Conference on Intelligent System Design and Engineering Application (ISDEA), IEEE, pp 1113–1116